Lumped methodology applied to sensible thermal storage systems

Andriotty Tiago H.[a], Rodrigues Letícia J [b] , Rocha Luiz A.O [c] and Schneider Paulo S [d]

Department of Mechanical Engineering, Federal University of Rio Grande do Sul, Porto Alegre - Brazil,
[a] tiago.haubert@ufrgs.br, [b] leticia.jenisch@mecanica.ufrgs.br, [c] laorocha@gmail.com, [d] pss@mecanica.ufrgs.br

Abstract:
This study applies a Lumped methodology to evaluate the behavior of a sensible thermal storage system subjected to cyclic energy source. Flat plates with the storage medium are assembled face to face and submitted to a parallel air stream. The storage medium is modeled as a Lumped system and the fluid by a non capacitive energy balance. The dimensions of the storage elements are limited to the range of validity of the modeling approach, as a function of the Biot number. Two cases are proposed, considering two storage materials (granite and AISI304 steel) with different geometries, air flow rates and volumes. Results from the Lumped model are compared to simulations performed on a commercial CFD code, and deviations remain in the order of 8% for steel and 3% for granite, when the system reaches a periodic stabilized condition.

Keywords:
Thermal storage, sensible heat storage, Lumped model, cyclic energy storage

1. Introduction

Among the renewable sources, solar energy is recognized as one of the most promising ones, mainly because it is abundant, free and environmentally clean. However, solar energy is intermittent, seasonal and varies according to local conditions. Thus, its storage can play a special role whenever the system is meant to operate under continuous and stable conditions. Energy accumulators can reduce the time delay between demand and supply, thereby improving the system performance.

In this context, the study of Thermal Energy Storage (TES) systems is gaining strength today. Published reviews [1-3] on TES systems classify the Heat Storage Materials (HSM) in two main groups: sensible and latent HSM, or PCM. In a general view, HSM must be chemically stable, with high thermal conductivity and high storage capacity, which means high density combined to high specific heat, non-toxic and non-corrosive. Latent HSM, must also display high phase change enthalpies together with small volume variation along the phase change.

Chauhan et al. [4] developed a numerical code to evaluate a coriander solar dryer. Two cases were assessed: in the first case, the drying process was performed without any storage system, while in the second one, rocks were used as HSM. The objective was to reduce the coriander moisture from 28,2% to 11,4%. Results indicated 27 sunshine hours (3 days) for the first case and 31 cumulative hours, including the night period, for the second case.

Sragovich [5] optimized a high temperature heat storage system for Solar Thermochemical Pipeline System. The author adapted the methodology proposed by Duffie and Beckman [9], based on a Lumped approach to evaluate the HSM coupled to an energy balance applied to the working fluid. The objective was to sustain the system air temperature above 900°C along cloud periods for at least 30 min. The optimization focused the geometry of the heat exchanger and attained the operational.

Salomoni et al. [6] proposed two different numerical methodologies to design a sensible TES with tubular channels inside concrete blocks for solar power plants, with water as the working fluid. The

HSM model was solved by a finite element numeric approach, and the heat transfer along the interface with the working fluid was modelled by convective correlations. In the first methodology, named “quasi-steady”, the fluid was modelled in one unique control volume and its transient term was neglected. The second one, named “non-steady”, discretised the fluid in several volumes, following Sragovich [5]. Similar results were obtained by both models whenever the tube length did not exceed 10 m. In this case, authors suggested that the “quasi-steady” model was more indicated, since it demanded less computational effort. For longer tubes, the “non-steady” model generated better results.

Based on that review, the objective of the present investigation is to compare the transient behaviour of a sensible thermal energy storage system obtained by CFD code to the one modelled by a Lumped methodology.

2. Heat transfer modelling

2.1 Lumped model (LPM)

The Thermal Storage System (TES) was composed by a Heat Storage Material (HSM) and air as the working fluid. The HSM was disposed in parallel flat plates and air flowing within them (Figure 1).

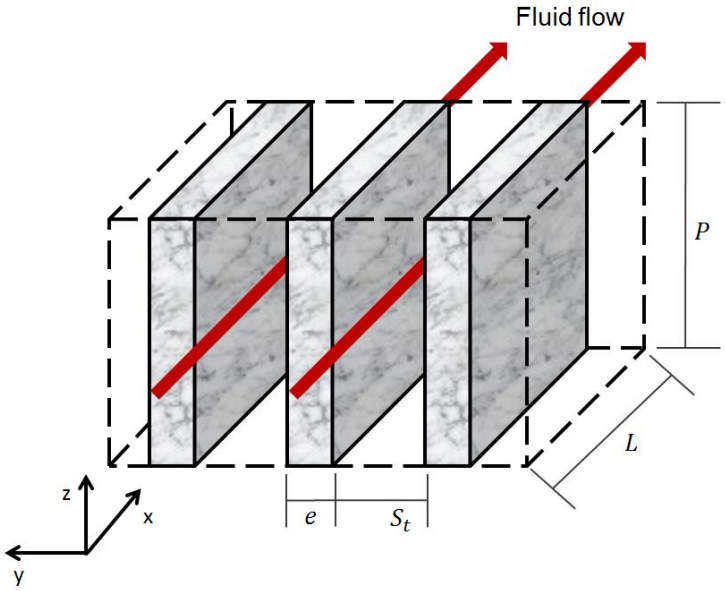

Fig. 1. Schematic view of the Thermal Energy Storage (TES).

The modeling is written for a single plate, with a control volume that is based on the symmetry of the system Fig (2.a). The energy balance takes into account half of the plate width *e/2* and half of the air channel width $S_t/2$ that shared a common interface. The opposites borders were considered as adiabatic.

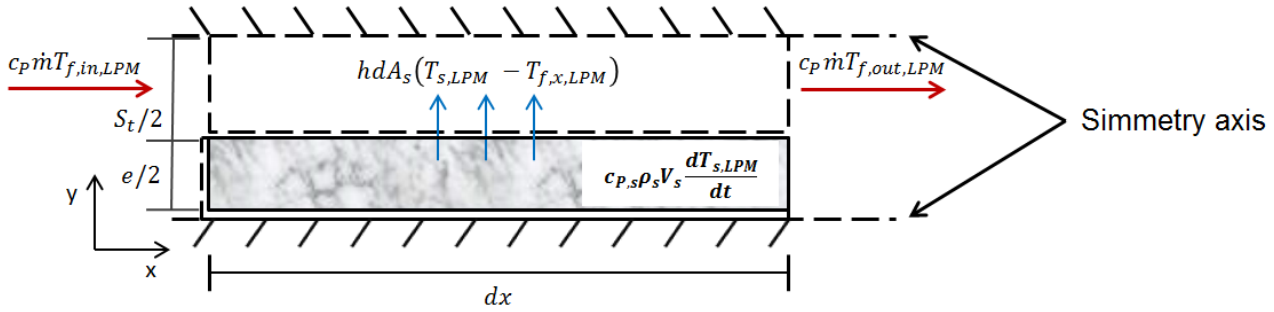

Fig. 2. Energy balance based on the control volumes for the Heat Storage Material (HSM) and air

The Lumped approach is based on the assumption that the temperature gradients in the storage material can be neglected whenever the medium displays a high thermal conductivity or the heat exchange along its interface with the working fluid is low, or a combination of both. Therefore, the temperature of the solid medium surface $T_{s,LPM}$ can be considered as uniform. These conditions allow presenting the energy balance as:

$$-hA_s(T_{s,LPM} - T_{f,LPM}) = c_{p,s}\rho_s V_s \frac{dT_{s,LPM}}{dt} \quad (1)$$

The difference between the HSM and the working fluid temperatures is defined as a temperature excess θ^*,

$$\theta^* = T_{s,LPM} - T_{f,LPM} \quad (2)$$

Considering that the fluid temperature is uniform and constant, the θ^* time variation is expressed by $(d\theta^*/dt) = (dT_{s,LPM}/dt)$, and (2) is rewritten as

$$-hA_s\theta^* = c_{p,s}\rho_s V_s \frac{d\theta^*}{dt} \quad (3)$$

It is important to observe that the uniform and constant fluid temperature assumption is an approximation. It varies in space, as the fluid gives or receives energy from the HSM, and in time, as the HSM temperature varies. These considerations are discussed in section 2.1.

Appling the integrations limits and defining an initial excess solid temperature as $\theta^*_{s,0} = T_{s,0,LPM} - T_{f,LPM}$, equation (3) becomes

$$-\frac{hA_s}{c_{p,s}\rho_s V_s}\int_0^t dt = \int_{\theta^*_{s,0}}^{\theta^*} \frac{d\theta^*}{\theta^*} \quad (4)$$

The solution of (4) represents the HSM temperature $T_{s,LPM}$ over time *t*

$$T_{s,LPM} = T_{s,0,LPM} - \left[1 - exp\left(-\frac{hA_s}{c_{p,s}\rho_s V_s}t\right)\right]\left(T_{s,0,LPM} - T_{f,LPM}\right) \quad (5)$$

Next equation expresses the resulting fluid one-dimensional energy balance, by neglecting the variation on the fluid temperature along the *y* direction:

$$\dot{m}\, c_{p,f}\, T_{f,in,LPM} - \dot{m}\, c_{p,f}\, T_{f,out,LPM} + h\, A_s\left(T_{s,LPM} - T_{f,x,LPM}\right) = c_{p,f}\rho_f V_f \frac{dT_{f,x,LPM}}{dt} \quad (6)$$

As the fluid heat capacity is significantly smaller than the one of the HSM, the right hand term on (6) can be neglected. By expanding $A_s = Pdx$, where P is the plate width, the equation is rewritten as

$$\frac{hP}{c_{p,f}\dot{m}} = \frac{dT_{f,x,LPM}}{dx}\frac{1}{\left(T_{s,LPM} - T_{f,x,LPM}\right)} \quad (7)$$

By deriving (2) in respect to the *x*-direction and assuming that the medium temperature is uniform, it leads to the following expression:

$$\frac{d\theta^*}{dx} = -\frac{dT_{f,x,LPM}}{dx} \quad (8)$$

Defining the initial excess fluid temperature as $\theta^*_{f,0} = T_{s,LPM} - T_{f,in,LPM}$ and L as the length of the solid domain, the integration over the domain gives the following expression:

$$-\frac{hP}{c_{p,f}\dot{m}}\int_0^L dx = \int_{\theta^*_{f,0}}^{\theta^*}\frac{d\theta^*}{\theta^*} \quad (9)$$

The solution of Equation 9, for the fluid temperature leaving the control volume, $T_{f,out,LPM}$, for a given length L is

$$T_{f,out,LPM} = T_{s,LPM} - \left[\exp\left(-\frac{hP}{c_{p,f}\dot{m}}L\right)\left(T_{s,LPM} - T_{f,in,LPM}\right)\right] \quad (10)$$

Equations (5) and (10) model the HSM and the working fluid. It is worth noticing that solid and fluid temperatures vary exponentially (solid over time and fluid over *x*-direction).

2.2 Model limitations

Equation (5) was obtained by considering that the fluid temperature $T_{f,LPM}$ was uniform, which is not exact, as it becomes a function of the length, $T_{f,x,LPM}$, as appears in (6). The fluid temperature $T_{f,x,LPM}$varies along the wall channel, kept at constant temperature $T_{s,LPM}$, as indicated in Figure 3:

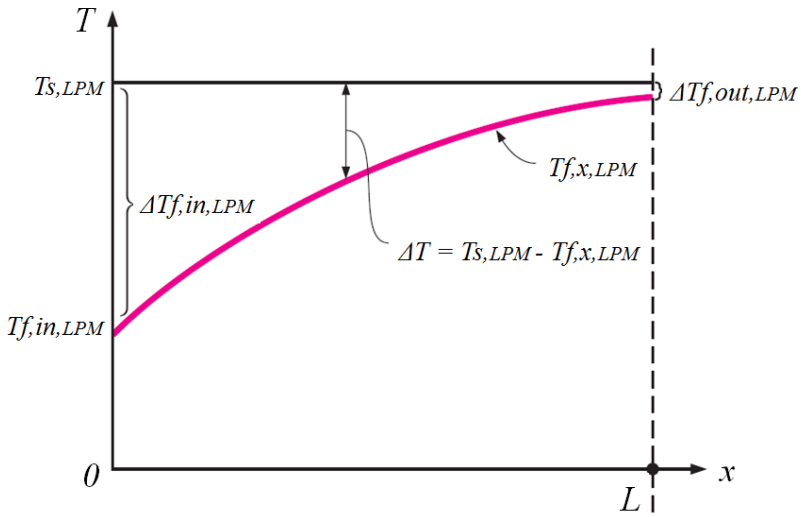

Fig. 3. Fluid temperature profile along a channel at constant wall temperature (adapted from [7]).

The fluid temperature $T_{f,LPM}$ that appears in (5) is expressed as the arithmetic mean of the inlet and outlet fluid temperatures, in order to simplify the formulation. According to Çengel [7], if the difference between $\Delta T_{f,in,LPM}$ and $\Delta T_{f,out,LPM}$ is less than 40%, the deviation using arithmetic mean approximation is lesser than 1%.

It is possible to observer in (5) that the arithmetic mean of the fluid temperature varies along time, as a function of the HSM behaviour, witch leads to the time discretization of equations (5) and (10). The solid medium displays a volumetric thermal capacity 3 times higher than the one of the air (tables 1 and 3), meaning that the inertial response of the solid is slower than the one of the air. Simulation performed with small time steps showed little variations on the HSM temperature, allowing to consider it as constant, as well as the arithmetic mean of the fluid temperature, for a given period of time.

Besides this consideration, the Lumped model is limited to low conductive resistance R_{cond} to convective resistance R_{conv} ratios, given by the Biot number:

$$Bi = \frac{R_{cond}}{R_{conv}} = \frac{hL_c}{k_s} \tag{11}$$

To guarantee Biot number below 0.1, the original HSM length L was divided in n independent volume sections of length L/n, as proposed by Sragovich [5] and Duffie and Beckman [9], as shown in Fig. 4.

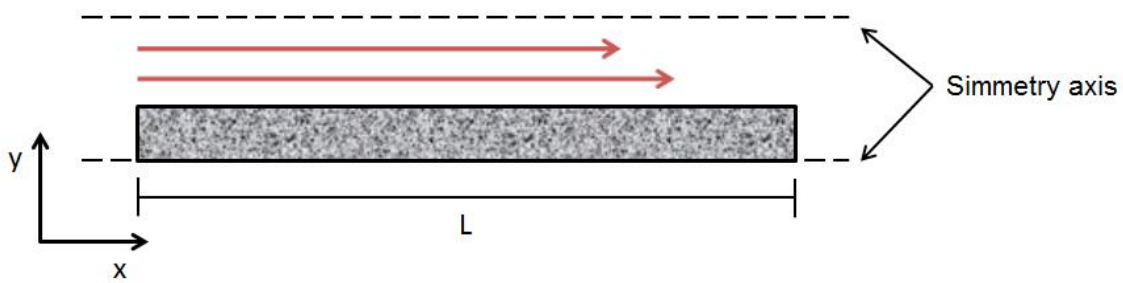

(a)

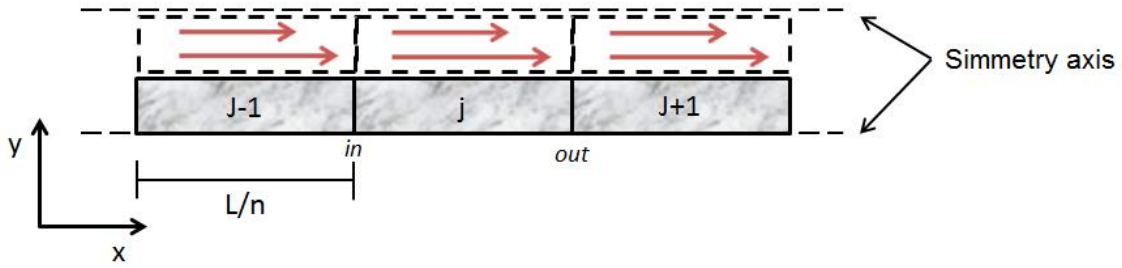

(b)

Fig. 4. Section scheme proposed by [5,9], (a) original system and (b) 3 independent and insulated plates.

The characteristic length L_c in (11) is commonly defined as the ratio between the solid volume and its surface area. Considering that both the working fluid temperature and the superficial heat transfer coefficient vary along the TES domain in a non-fully developed flows, the heat transferred between fluid and solid is not constant along the channel length. A new characteristic length $L_{c,n}$ is then defined as the geometrical distance between the points of maximum temperature difference along the solid medium, shown in Figure 5, allowing to expand the range of application of the Lumped approach for TES systems.

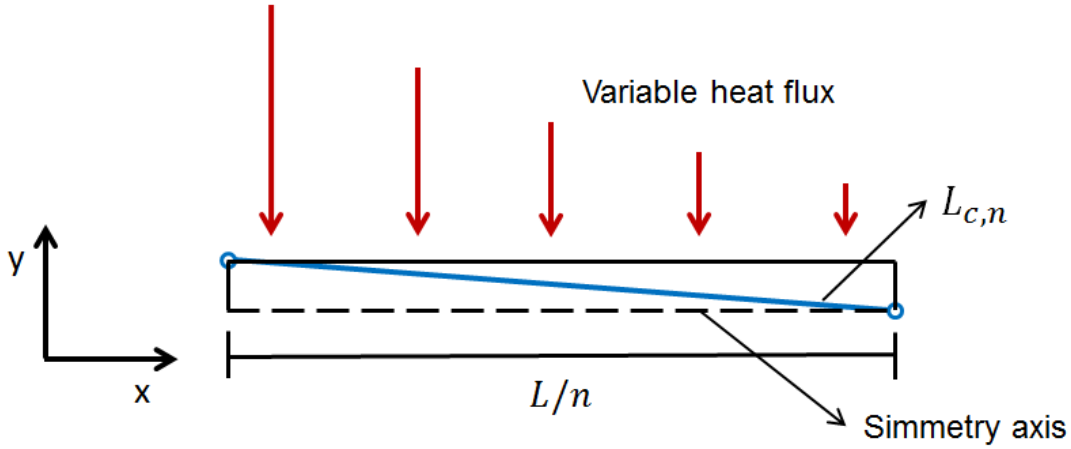

Fig. 5. Characteristic length $L_{c,n}$ based on extreme temperature difference.

These discretization in time and in space lead to rewrite equations (5) and (10) as follows:

$$T_{s,t,j,LPM} = T_{s,t-\Delta t,j,LPM} - \left[1 - exp\left(-\frac{hA_{s,j}}{c_{p,s}\rho_s V_{s,j}}\Delta t\right)\right]\left(T_{s,t-\Delta t,j,LPM} - \frac{T_{f,\mathrm{t,j,in},LPM} + T_{f,\mathrm{t,j,out},LPM}}{2}\right) \quad (12)$$

$$T_{f,\mathrm{t,j,out},LPM} = T_{s,t,j,LPM} - \left[\exp\left(-\frac{hP}{c_{p,f}\dot{m}}(L/n)\right)\left(T_{s,t,j,LPM} - T_{f,\mathrm{t,j,in},LPM}\right)\right] \quad (13)$$

where the solid and the air mean temperatures T_s and T_f are now expressed as a function of a time step Δt and a section j. The Lumped model for the TES is then composed by equations (12) and (13) and auxiliary by the restrictions given by Eq. (11)

3. Cases

The storage behavior of the TES depicted in Fig. (1) was simulated with the aid of the Lumped method for two HSM, with distinct thermophysical properties (Table 1).

Table 1. Thermophysical properties of the HSM [8]

Materials	Density ρ [kg/m³]	Specific heat c_p [J/(kgK)]	Thermal conductivity k [W/(mK)]	Thermal diffusivity [m² /s]	Volumetric heat capacity [J/(m³K)]
AISI 304 (steel)	7 900	477	14.90	3.95 E-6	3.76 E+6
Granite	2 630	775	2.790	1.36 E-6	2.03 E+6

These materials were chosen due to the differences on their thermophysical properties, together with its commercial availability.

Both cases were run for a total plate length L (Fig. (4. a)) of 0.3 m and HSM and air initial temperature of 320 K, generating the dimensional parameters displayed in Table 2, based on the restriction given by Eq. (11). Parameters as plate thickness, channel width and inlet air velocity were obtained by optimization, performed in a prior work [12], based on the minimization of the exchanged heat transfer rate in respect to a target value.

Table 2. TES Parameters for each of the simulation cases.

Parameters	Case A - AISI304	Case B - Granite
L/n [m]	0.1	0.01875
HSM and air initial temperature [K]	320	320
Plate thickness e [m]	0.015315	0.02033
Channel width [m]	0.00507	0.005085
Inlet air speed [m/s]	0.2578	0.7500

Air proprieties are displayed in Table 3.

Table 3. Air proprieties calculated in respect to an average temperature of 320 K [8].

Density ρ [kg/m³]	Specific heat c_p [J/(kgK)]	Dynamic Viscosity [kg/(ms)]	Prandtl Number [-]	Thermal conductivity k [W/(mK)]	Volumetric heat capacity [J/(m³K)]
1.103	1 008	1.949 E-5	0.705	2.785 E-2	1.111 E+3

The convective heat transfer h in equations (11), (12) and (13) was estimated after the correlation proposed by Stephan [10], *apud* Bejan [11], for laminar fluid flow through an infinite parallel flat plates with a characteristic length D_h given by the hydraulic diameter.

$$\overline{Nu}_{D_h} = \frac{h\,D_h}{k_f} = 7.55 + \frac{0.024 L_*^{-1.14}}{1 + 0.0358 Pr_f^{0.17} L_*^{-0.64}} \quad \text{with } L_* = \frac{L}{D_h Re_{D_h} Pr_f} \tag{14}$$

The TES inlet air temperature $T_{\infty.t}$ was predicted by Eq. (15).

$$T_{\infty.t} = T_{\infty.min} + \left[1 + sen\left(\frac{\pi t}{\beta}\right)\right]\left(\frac{T_{\infty.max} - T_{\infty.min}}{2}\right) \tag{15}$$

with air extreme temperatures of $T_{\infty.min}$ = 290 K and $T_{\infty.max}$ = 350 K. This simple sine wave expression can represent cyclic behaviours in storage systems.

Simulations with the Lumped model were performed with the aid of an algebraic solver (*EES*) for 4 cycles of β = 20 000 seconds each. Results were compared to the ones from the software *COMSOL*, capable of solving the coupled equations of continuity, Navier-Stokes, and energy for the fluid *f*, and the energy equation for solid domain *s*, as follows

$$\nabla \cdot \boldsymbol{u}_f = 0 \tag{16}$$

$$\rho_f(\boldsymbol{u}_f \cdot \nabla)\boldsymbol{u}_f = -\boldsymbol{\nabla} p_f + \mu_f(\nabla^2 \boldsymbol{u}_f) \tag{17}$$

$$\rho_f C_{p,f} \frac{\partial T}{\partial t} + \rho_f C_{p,f} \boldsymbol{u}_f \cdot \nabla T_f = k_f \nabla^2 T_f \tag{18}$$

$$\rho_s C_{p,s} \frac{\partial T_s}{\partial t} = k_s \nabla^2 T_s \tag{19}$$

COMSOL was run for a transient two-dimensional geometry (*x*-*y*) and results were compared in terms of an effective temperature $T_{eff,CFD}$, based on the rate of thermal energy integrated over the cross section area, as defined by [8]:

$$T_{eff,CFD} = \frac{\int_{A_c} \rho_f u c_{p.f} T_f d\, A_c}{\dot{m} c_{p.f}} \tag{20}$$

COMSOL is based on a finite element scheme, and automatically generated a triangular mesh, according to the physics of the problem (more refined in the fluid domain, and lesser in the solid). The mesh for Case A was built by 180 218 elements and for Case B by 126 230 elements.

4. Results

Simulations were performed for the 2 cases presented earlier in this work by both the Lumped method and CFD approach. Results from these 2 numerical schemes were compared for the behavior of the TES outlet air temperature and then for the exchanged heat to the air flow.

4.1 TES outlet air temperature

Fig. (6) displays the arithmetic difference between the outlet fluid temperatures obtained by both approaches, given by $T_{eff,out,CFD} - T_{f,out,LPM}$, in respect to the total length *L*.

In both cases, results for the first 20 000 s showed smaller difference between the system outlet fluid temperature calculated by Lumped model and CDF code, if compared to the complete simulation. Both the HSM and the fluid temperatures were taken as 320 K at the begging of the run, meaning that along the first 20 000 seconds, the Nusselt numbers were smaller. After reaching the stable cyclic condition, both cases showed similar behaviour in regard to the fluid temperatures difference at the system outlet. Figure 6 shows that this difference in Case B was higher than in Case A.

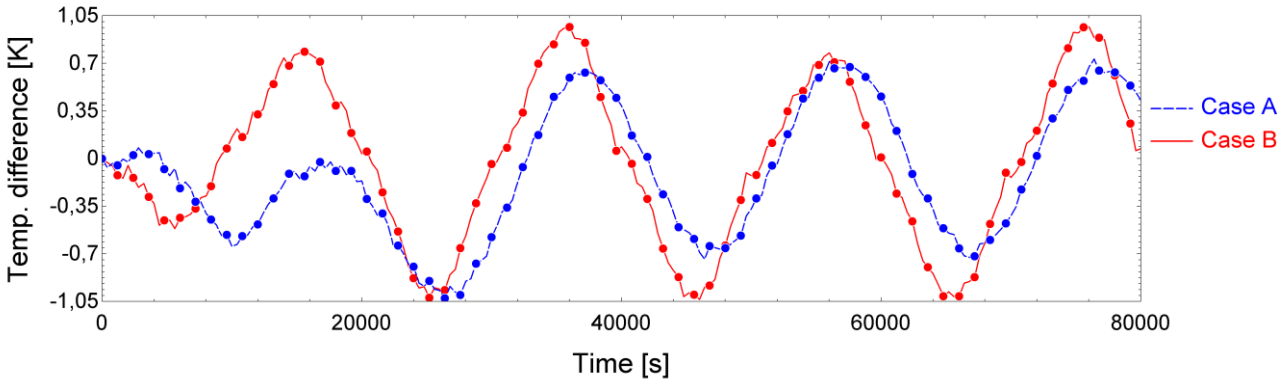

Fig. 6. Arithmetic difference between the outlet fluid temperature calculated by the CFD code and the Lumped model, $T_{eff,out,CFD} - T_{f,out,LPM}$, for Case A – Steel and Case B – Granite.

4.2 Exchanged heat to the air flow

The overall exchanged heat $Q_{LPM_{t+\Delta t}}$, in J, from the solid to the fluid was calculated by the Lumped method as the summation given by (21) as:

$$Q_{LPM_{t+\Delta t}} = \sum_{t=1}^{t=Nts}\left[\left(c_{p,s}\rho_s\frac{V_s}{n}\right)\sum_{j=1}^{j=n}\left(\left|T_{s,t+\Delta t,j,LPM} - T_{s,t,j,LPM}\right|\right)\right] \quad (21)$$

with Nts the number of time steps.

The *COMSOL* software was capable to perform an equivalent computation with the aid of an internal function called "total heat flux, y component", integrated along the surface area A_s, represented by Q_{CFD_t}, em J

Results were assessed by means of the relative $D_{rel}(\%)_t$, proposed as:

$$D_{rel}(\%)_t = \sum_{t=1}^{t=Nts}\left(\frac{\left|Q_{CFD_t} - Q_{LPM_t}\right|}{Q_{CFD_t}}\right)100 \quad (22)$$

for a given time step *t*. Figure 7 shows the deviation behavior for a simulation limit of *Nts=200*.

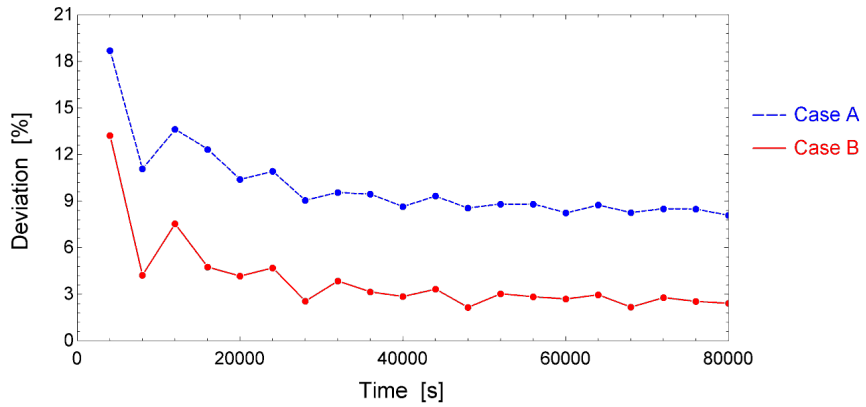

Figure 7: Relative heat transfer deviation (equation 22) calculated by the CFD code and the Lumped approach for Case A – Steel and Case B – Granite.

For both cases, the relative deviations were higher for the first 20 000 seconds, starting with 19% for Case A and 13% for Case B. In that case, Nusselt numbers were smaller if compared to the complete simulation. As a consequence, small deviations on the fluid temperature resulted in higher deviations between heat transferred in the Lumped model and the CFD code.

After this period, the relative deviation reached steady values of 8% for Case A and 3% for Case B, approximately, at the same time that the TES system reached stabilized operational conditions.

The Biot numbers were estimated as 0.075 for Case A and 0.120 for Case B, and besides de fact that this last value is higher than the first one, Case B deviation was smaller than in Case A. This occurs because the approximation for the arithmetic mean of the fluid temperature is more accurate when the difference between the section inlet and outlet fluid temperature is smaller (according to Fig. 3). More sections and higher mass flow rate can decrease this difference, improving the results from the Lumped model.

5. Conclusions

The Lumped approach applied to the TES system presented higher heat transferred deviation when the system is not stabilized. This relative deviation decreased when the simulation reached a cycled regime, remaining around 8% for Case A and 3% for Case B. Case B showed smaller deviations, even with higher Biot number than Case A, due to fluid flow conditions (higher mass flow rate) and higher number of sections. Both characteristics resulted in a better approximation of the arithmetic mean fluid temperature, improving the Lumped model results. Smaller Nusselt numbers increased the Lumped model errors, since even small variations on the fluid temperature had a significant influence on the total heat transferred between the HSM and fluid.

Nomenclature

A surface area, m^2

Cp specific heat, J/(kgK)

D_h hydraulic diameter, m

D_{rel} diviation, %

h heat transfer coefficient, $W/(m^2K)$

k thermal conductivity, W/(mK)

L plate length, m

L_c characteristic length, m

$\dot{m}$ mass flow rate, kg/s

Nts number of time steps

n number of sections

p pressure, Pa

P plate width, m

Pr_f fluid Prandtl number

Q total heat transferred, J

Re_{D_h} Reynolds number based on the hydraulic diameter

T Temperature, K

t time, s

u fluid flow velocity, m/s

V volume, m^3

Greek symbols

ρ density, kg/m^3

θ^* excess temperature, K

μ Dynamic viscosity, kg/(ms)

Δt time step, s

∇ nabla operator

β sin cycle period, s

Subscripts and superscripts

c channel cross section

CFD Computational Fluid Dynamics

eff effective

f fluid

in inlet

j section

LPM Lumped Model

0 initial

out outlet

s solid

x x-direction

Acknowledgments

Smith Schneider acknowledges CNPq (PQ 305357/2013-1).

References

[1] HASNAIN. S., Review on sustainable thermal energy storage technologies. part i: heat storage materials and techniques. Energy conversion and management. V. 39. n. 11. p. 1127-1138. Aug 1998. ISSN 0196-8904.

[2] BAL. L.; SATYA. S.; NAIK. S., Solar dryer with thermal energy storage systems for drying agricultural food products: a review. Renewable & sustainable energy reviews. V. 14. n. 8. p. 2298-2314. Oct 2010. ISSN 1364-0321.

[3] CABEZA. L.; CASTELL. A.; BARRENECHE. C.; GRACIA. A.; FERNÁNDEZ. A. I., Materials used as PCM in thermal energy storage in buildings: a review. Renewable & sustainable energy reviews. V. 15. n. 3. p. 1675-1695. Apr 2011. ISSN 1364-0321.

[4] CHAUHAN. P.; CHOUDHURY. C.; GARG. H., Comparative performance of coriander dryer coupled to solar air heater and solar air-heater-cum-rockbed storage. Applied thermal engineering. V. 16. n. 6. p. 475-486. Jun 1996. ISSN 1359-4311.

[5] SRAGOVICH. D., Transient analysis for designing and predicting operational performance of a high-temperature sensible thermal-energy storage-system. Solar energy. V. 43. n. 1. p. 7-16. 1989. ISSN 0038-092X.

[6] SALOMONI. V.; MAJORANA. C.; GIANNUZZI. G.; MILIOZZI. A.; MAGGIO. R.; GIRARDI. F.; MELE. D.; LUCENTINI. M., Thermal storage of sensible heat using concrete modules in solar power plants. Solar energy. V. 103. p. 303-315. May 2014. ISSN 0038-092X.

[7] ÇENGEL. Y. A., Heat Transfer: A Practical Approach. 2nd ed.. McGraw-Hill. 2002. ISBN 978-0-072-45893-0.

[8] INCROPERA F. P.; DEWITT D. P., Fundamentals of Heat and Mass Transfer. 7th ed.. New Jersey. John Wiley & Sons. INC.. 2011. ISBN 978-0-470-91323-9.

[9] DUFFIE J. A.; BECKMAN W. A., Solar Engineering of Thermal Processes. New York. John Wiley & Sons. INC.. 4th edition. 2013. ISBN 978-0-470-87366-3

[10] STEPHAN K., Wärmeübergang und Druckabfall bei nicht ausgebildeter Laminarströmung in Röhren und ebenen Spalten. Chen. Int. Tech.. Vol. 31. 1959. pp. 773-778.

[11] BEJAN A., Convection Heat Transfer. New Jersey. John Wiley & Sons. INC.. 2004. ISBN 978-0-470-90037-6.

[12] ANDRIOTTY T. H., Structures optimization for sensible heat accumulation (in Portuguese), Master thesis, Universidade Federal do Rio Grande do Sul, 2014.